Research Square

Preprints are preliminary reports that have not undergone peer review.
They should not be considered conclusive, used to inform clinical practice,
or referenced by the media as validated information.

Deep Learning Based Automated Histological Diagnosis of Eosinophilic Chronic Rhinosinusitis and Clinical Correlation

Jae Yoon Lee
The Catholic University of Korea
Hyeokjin Kweon
Korea Advanced Institute of Science and Technology (KAIST)
David Jang
Duke University School of Medicine
Keonhyeok Park
Pohang University of Science and Technology (POSTECH)
Do Hyun Kim
dohyuni9292@naver.com
The Catholic University of Korea
Seungchul Lee
Korea Advanced Institute of Science and Technology (KAIST)

Article

Keywords:

Posted Date: June 19th, 2026

DOI: https://doi.org/10.21203/rs.3.rs-9764769/v1

License: This work is licensed under a Creative Commons Attribution 4.0 International License.
Read Full License

Additional Declarations: No competing interests reported.

Abstract

Eosinophilic chronic rhinosinusitis (ECRS) diagnosis relies on tissue eosinophil counts, but manual counting is labor intensive and subject to interobserver variability. To develop a deep learning model for automated eosinophil quantification from histologic images and evaluate its clinical correlation with ECRS diagnosis In this retrospective study, 41 nasal polyp patients who underwent ESS were included. Deep learning was applied to H&E-stained slides to estimate the eosinophil count per high-power field (HPF). Model performance was assessed using receiver operating characteristic (ROC) curve analysis, and the correlation with the JESREC score was analyzed using Pearson correlation and linear regression. Among the cohort, 16 patients (39.0%) were diagnosed with ECRS. The model achieved an AUC of 0.979 (95% CI: 0.945–1.000), indicating high diagnostic accuracy. The optimal diagnostic threshold was identified at 42 eosinophils/HPF. A significant positive correlation was observed between estimated eosinophil count and JESREC score ($r = 0.645$, $p < 0.001$). Regression analysis yielded the following equation: JESREC = 0.100 × eosinophil count + 6.810. This deep learning-based eosinophil counting tool offers an accurate, objective, and rapid method for the histopathological diagnosis of ECRS. It has the potential to enhance clinical decision-making and streamline diagnostic workflows in chronic rhinosinusitis care.

Introduction

The precise diagnosis of eosinophilic chronic rhinosinusitis (ECRS) is important for clinicians, as early identification can be used to determine prognosis[1], and the accurate identification of tissue eosinophilia is crucial for clinical decision-making, as it directly affects treatment strategies, including the selection and timing of systemic steroids and biological agents, which critically influence recurrence rates and quality of life for ECRS patients[2]. Moreover, distinguishing ECRS from noneosinophilic variants helps predict disease severity, surgical outcomes, and the likelihood of polyp recurrence, making precise eosinophil quantification essential for personalized patient management[3].

Deep learning has revolutionized histopathological analysis across multiple medical disciplines over the past decade[4]. Artificial intelligence (AI) models have achieved expert-level performance in detecting breast cancer metastases in lymph nodes, grading prostate cancer, and identifying molecular subtypes of lung adenocarcinoma[5–7]. Deep learning algorithms have also demonstrated accuracy in diagnosing eosinophilic esophagitis, assessing inflammatory activity in ulcerative colitis, and detecting early gastric neoplasia[8]. These applications have not only matched pathologist-level accuracy but also reduced the diagnostic time from hours to seconds while providing consistent, reproducible results free from interobserver variability.

Despite these technological advances in digital pathology, the diagnosis of ECRS remains dependent on manual histopathological evaluation[9]. In current practice, pathologists need to manually identify and count eosinophils in multiple high-power fields—a labor-intensive process that is both time consuming and prone to human error. Furthermore, this conventional approach faces significant limitations:

pathologists typically examine only selected inflammatory hotspots (usually three high-power fields), which may not represent the overall tissue eosinophil burden[10].

Automated analysis can evaluate entire tissue sections rather than selected fields, providing a more comprehensive assessment of eosinophil distribution and density. This whole-slide approach eliminates selection bias while dramatically reducing analysis time—enabling the evaluation of multiple slides within seconds rather than the minutes or hours required for manual counting. The reproducibility of AI-generated results ensures diagnostic consistency, which is particularly valuable given that ECRS diagnosis often requires the counting of dozens to hundreds of eosinophils across multiple fields. Moreover, such technology could democratize access to expert-level histopathological analysis in resource-limited settings where specialized pathologists may not be readily available.

We present a deep learning-assisted method to precisely quantify eosinophils in histological images of nasal polyps. With standard hematoxylin and eosin (H&E)-stained tissue sections, our model enables any clinician to obtain accurate, reproducible eosinophil counts within seconds in the clinical setting. This automated approach not only streamlines the diagnostic workflow but also provides objective, quantitative data that correlate with clinical disease severity, thereby supporting evidence-based treatment decisions for ECRS patients.

Results

Baseline characteristics

A total of 41 patients with nasal polyps were evaluated. Among these patients, 16 (39.0%) were diagnosed with ECRS. Asthma was present in 12 patients (29.3%). Table 1 provides a breakdown by group. The mean age was comparable between ECRS (45.5 ± 17.2 years) and non-ECRS (43.6 ± 21.1 years) patients. A male predominance was noted in the ECRS group (56.2%); in the non-ECRS group, 44.0% of the patients were male.

Table 1. Characteristics of the Patient Population

Sex	All subjects (N = 41)	ECRS (n = 16)	Non-ECRS (n = 25)
Male	20 (48.8%)	9 (56.2%)	11 (44.0%)
Female	21 (51.2%)	7 (43.8%)	14 (56.0%)
Age (years)	44.3 ± 19.5	45.5 ± 17.2	43.6 ± 21.1
History of Asthma	12 (29.3%)	6 (37.5%)	6 (24.0%)
CT (Lund-Mackay Score)			
Maxillary sinus	1.07 ± 0.53	1.16 ± 0.44	1.02 ± 0.59
Anterior ethmoid sinus	1.24 ± 0.65	1.56 ± 0.48	1.04 ± 0.68
Posterior ethmoid sinus	1.16 ± 0.71	1.59 ± 0.46	0.88 ± 0.71
Frontal sinus	1.05 ± 0.82	1.28 ± 0.71	0.90 ± 0.87
Sphenoid sinus	0.63 ± 0.72	0.84 ± 0.70	0.50 ± 0.72
Ostiomeatal complex	1.20 ± 0.69	1.28 ± 0.71	1.14 ± 0.68
Total sum	6.21 ± 3.67	7.81 ± 3.04	5.18 ± 3.72
Olfactory cleft	0.73 ± 0.78	1.06 ± 0.85	0.52 ± 0.67
Ethmoid/Maxillary ratio	1.49 ± 0.85	1.72 ± 0.77	1.34 ± 0.89
Posterior/Anterior ethmoid ratio	0.98 ± 0.29	1.05 ± 0.23	0.94 ± 0.33
Serum eosinophil (%)	4.36 ± 3.82	7.34 ± 4.16	2.45 ± 1.94
Serum eosinophil count (cells/μL)	280.05 ± 258.28	487.59 ± 271.53	147.22 ± 134.17
ECP (ng/mL)	56.45 ± 41.93	77.20 ± 42.63	43.16 ± 36.38
Butanol threshold test	9.47 ± 4.55	8.81 ± 4.42	9.89 ± 4.68
Smell identification test	6.66 ± 2.59	6.38 ± 2.87	6.84 ± 2.44

ECRS, eosinophilic chronic rhinosinusitis; the table shows the mean and standard deviation for continuous variables, number (%) for binary variables, and the number per group for categorical variables. Lund-Mackay scores of both sinuses were added, and the presence of an Olfactory cleft was scored as 0 if absent, 1 if partial, and 2 if total opacification was present. Ratios on CT were calculated as the means of both sides.

Dataset and Image Preprocessing

Histological images were obtained from 41 patients. Among these, 31 patients—16 with ECRS and 15 without—constituted the training dataset; the remaining 10 patients (5 with ECRS and 5 without ECRS) constituted the validation set. All the images were resized to 640 × 640 pixels to standardize the spatial resolution across the samples. To improve the generalizability of the model, two geometry-based augmentations—horizontal and vertical flipping—were applied with equal probability to every training image; no color or intensity augmentations were used to preserve histochemical fidelity.

Evaluation Metrics

Model performance was quantified with four common object-detection metrics. First, precision (P) expresses the proportion of algorithmic detections that are true eosinophils and is defined as follows:

$$\mathrm{P} = \frac{\mathrm{TP}}{\mathrm{TP} + \mathrm{FP}}$$

where TP and FP stand for true positives and false positives, respectively. Second, recall (R), the fraction of true eosinophils that the model successfully detects, is defined as follows:

$$\mathrm{R} = \frac{\mathrm{TP}}{\mathrm{TP} + \mathrm{FN}}$$

where FN stands for false-negatives.

To summarize both precision and recall into a single metric, we also report the F1 score, defined as the harmonic mean of precision and recall:

$$\mathrm{F1} = \frac{2 \cdot \mathrm{P} \cdot \mathrm{R}}{\mathrm{P} + \mathrm{R}}$$

This score provides a balanced measure of the detection accuracy of a model, particularly in cases of class imbalance.

In addition, localization quality was assessed with the intersection over union (IoU), which was computed for every predicted versus annotated bounding box as the ratio of their overlap area to their union area. Using IoU, the average precision (AP) was obtained as the area under the precision–recall curve at a specified IoU threshold. We report the mean average precision (mAP) under two regimes: mAP@0.50, which averages AP when IoU ≥ 0.50, and mAP@0.50:0.95, which averages AP over ten thresholds from 0.50 to 0.95 in 0.05 increments:

$$\mathrm{mAP}[0.50!:!0.95] = \frac{1}{10}\sum_{t=0}^{9} \mathrm{AP}_{0.50+0.05t\cdot}$$

Model Validation Results

The proposed EoS-YOLOv8 model achieved a precision of 0.590, a recall of 0.681, an mAP@0.50 of 0.643, and an mAP@0.50:0.95 of 0.325 on the validation dataset. These values indicate that approximately 59% of all the predicted eosinophils were true positives, whereas nearly 68% of all the eosinophils present in the images were successfully detected by the model. The mAP scores, particularly the stricter mAP@0.50:0.95, show that the predicted bounding boxes remained well aligned with the ground truth (GT) even under tight IoU requirements, demonstrating reliable localization in densely populated microscopic fields. Qualitative examples of these detections are provided in Fig. 1, while the corresponding learning curves are shown in Fig. 2.

Notably, owing to the practical limitations of exhaustive manual annotation, some eosinophils may have been missed during GT labeling. As such, the reported recall and mAP values may underestimate the actual detection capability of the model. Despite this, the model consistently detected eosinophil-rich regions, suggesting its potential utility in assisting pathologists with quantitative tissue analysis.

Accuracy of the model for diagnosing ECRS

The deep learning model demonstrated excellent classification performance. As depicted in Fig. 3, the ROC curve yielded an AUC of 0.979 (95% CI: 0.945–1.000), indicating high diagnostic accuracy. The ideal diagnostic threshold was identified at 42 eosinophils per HPF, which was derived from the minimal value of the discriminant function $(1 - \text{sensitivity})^2 + (1 - \text{specificity})^2$. This threshold achieved an optimal balance between sensitivity and specificity in distinguishing ECRS.

Correlations between automated eosinophil counts and JESREC scores

The estimated eosinophil count from the model was significantly correlated with the JESREC score ($r = 0.645$, $p < 0.001$). Linear regression indicated a predictive relationship between eosinophil count and clinical disease severity, yielding the following equation: JESREC = 0.100 × eosinophils + 6.810 ($p < 0.001$).

Discussion

In this study, we developed and validated a model for automated eosinophil detection in nasal polyp histology, achieving high diagnostic performance and an optimal threshold of 42 eosinophils per HPF for ECRS. Importantly, the counts were strongly correlated with JESREC clinical severity scores, establishing a quantitative link between the histopathological findings and clinical disease burden [19]. These results represent the first successful application of deep learning to generate absolute eosinophil counts from nasal biopsy slides with direct clinical correlation.

Our model architecture incorporates several key innovations that enable reliable eosinophil detection despite the challenges of densely clustered cells and morphological variations. By integrating high-resolution feature branches, a CBAM and a BiFPN can effectively preserve fine-grained cellular details while leveraging contextual information from deeper layers. This design achieved strong localization accuracy even at stringent IoU thresholds, demonstrating reliable separation of densely packed eosinophils with minimal overmerging or false-positive artifacts. Despite these architectural additions, our modified model maintains computational efficiency with only 194 layers and 421,507 parameters—substantially smaller than the conventional model (224 layers, 11.2 million parameters). This lightweight design enables whole-image inference in approximately 17.9 milliseconds, representing an approximately 30,000-fold speed improvement over manual annotation, which typically requires 10 minutes per image.

The ability of the model to evaluate entire tissue sections addresses a fundamental limitation of current diagnostic practice. Traditional manual counting relies on the subjective selection of three typically high-inflammatory regions, introducing systematic bias that our validation results help quantify. As shown in Table 2, the results indicate that the precision is relatively low compared with the recall. This discrepancy can be partially attributed to the fact that the GT annotations were manually obtained by human experts. Since it is practically impossible to count every single eosinophil during manual labeling, some eosinophils detected by the AI model might not have been annotated and are therefore treated as false positives. For example, in patient ECRS-01, the model detected 61 out of 74 eosinophils annotated by the experts and identified 66 additional eosinophils that were not labeled by the annotators. Despite this discrepancy, the high recall values indicate that the model successfully detected the majority of the eosinophils annotated by human observers. Furthermore, the results for non-ECRS samples indicate that the model can effectively distinguish between ECRS and non-ECRS samples. This suggests that the model is not only robust to annotation variability but also capable of identifying previously unlabeled eosinophils that were overlooked during manual counting. By processing all fields and averaging counts across the entire image, our approach provides a more representative assessment of tissue eosinophil burden, potentially explaining the strong correlation with clinical severity scores.

Table 2. Per-image eosinophil detection metrics (IoU threshold = 0.5, confidence threshold = 0.3).

ECRS-01	GT	TP	FP	FN	Precision	Recall	F1-score
	74	**61**	**66**	**13**	**0.480**	**0.824**	**0.607**
ECRS-02	49	30	21	19	0.588	0.612	0.600
ECRS-03	137	109	66	28	0.623	0.796	0.699
ECRS-04	189	113	66	76	0.631	0.598	0.614
ECRS-05	15	7	8	8	0.467	0.467	0.467
Non-ECRS-02	2	1	0	1	1.000	0.500	0.667
Non-ECRS-04	2	2	1	0	0.667	1.000	0.800

No eosinophils were present in either the GT or predictions for NonECRS-01, NonECRS-03, or NonECRS-05. Abbreviations: IoU, intersection over union; GT, ground truth; TP, true positive; FP, false positive; FN, false negative.

Comparisons with previous AI applications in nasal polyp analysis highlight the unique contribution of our quantitative approach. Wang et al. developed a deep learning model for identifying histologic patterns predictive of poor prognosis in nasal polyps, emphasizing pathologic subtyping rather than eosinophil quantification[20]. While their model recognized eosinophil infiltration as a key prognostic marker, it did not provide actionable cell counts for diagnostic decision-making. Wu et al. performed whole-slide analysis to classify inflammatory cell types, generating composition ratios of eosinophils, lymphocytes, and neutrophils[21]. However, their categorical approach lacked correlation with clinical severity indices such as VAS, Lund-Kennedy, or Lund-Mackay scores. Our continuous numeric output directly addresses this gap, enabling nuanced clinical decisions regarding systemic steroid or biologic therapy on the basis of precise eosinophil burden.

The diagnostic threshold of 42 eosinophils/HPF identified through ROC analysis warrants careful interpretation within the broader context of ECRS diagnosis. This threshold achieved an optimal sensitivity–specificity balance in our cohort but should not be considered a universal benchmark given the known variation in diagnostic criteria across institutions and populations. The proximity of the threshold to commonly cited values suggests biological validity, yet standardization remains essential for widespread clinical adoption. Future integration with complementary biomarkers such as blood eosinophil counts or serum IgE levels could enhance diagnostic precision through multimodal assessment. Partial manual annotation likely omitted some eosinophils, resulting in conservative recall and mAP estimates, whereas the single-class focus precluded simultaneous quantification for comprehensive assessment. In addition, the enlarged feature maps increased memory demand on embedded hardware, and the decision logic of the model, although aided by attention maps, still lacks full interpretability for clinical end-users.

Methods

Study design and histopathological subclassification

In this retrospective analysis, 41 patients who underwent endoscopic sinus surgery (ESS) at a single tertiary medical center from January 2021 to December 2023 for nasal polyps were analyzed. Patients were categorized into ECRS or non-ECRS groups on the basis of the number of eosinophils counted per high-power field (HPF) at ×400 magnification in the three areas most densely infiltrated by inflammatory cells. Two rhinology specialists independently counted eosinophils in these three areas, and the mean count from each field was calculated. The final value was determined through consensus between the two observers after discussion and was confirmed by one pathologist. The diagnostic threshold for ECRS was set at 10 eosinophils/HPF, in accordance with the EPOS/EUFOREA 2023 guidelines[11]. This study was approved by the Institutional Review Board of Seoul Saint Mary's Hospital, The Catholic University of Korea (IRB No. KC24WISI0797; "Clinical Diagnosis of Eosinophilic Chronic Rhinosinusitis"). All methods were performed in accordance with the relevant guidelines and regulations, including the Declaration of Helsinki. Informed consent was waived by the Institutional Review Board of Seoul Saint Mary's Hospital, The Catholic University of Korea given the retrospective design utilizing archived histopathological specimens and anonymized clinical data.

Clinical characteristics

Preoperative demographics, asthma history, blood test findings, and olfactory test results were collected. Olfaction was measured according to the butanol threshold test and cross-cultural smell identification test[12,13]. CT scans were evaluated based on the Lund–Mackay scoring system[14]. Additional calculations for the olfactory cleft, ethmoid-to-maxillary sinus score ratio, and posterior-to-anterior ethmoid sinus score ratio were performed, as previous studies have shown that these indices are related to ECRS[15].

Deep learning-based tissue eosinophil count

To perform automated detection and quantification of tissue eosinophils on H&E-stained nasal polyp slides, a customized object detection model was developed based on the YOLOv8 framework[16]. While conventional YOLO models are designed primarily for generic object detection tasks involving large-scale natural images, such architectures are not optimal for histopathological analyses of small cellular structures. Eosinophils, in particular, are typically small in size (often smaller than 20 μm), exhibit a dense eosinophilic cytoplasm, and contain bilobed or dumbbell-shaped nuclei.

To address this, we modified the baseline YOLOv8 structure to create a model specifically optimized for histologic eosinophil detection, referred to as EoS-YOLOv8. The model architecture was adapted into three major components: backbone, neck, and detection layer.

Within the feature-extracting backbone, we added an early-stage output branch that retains high-resolution spatial information, which is often lost in standard deep networks because of progressive downsampling. This approach allows the model to better capture the fine morphological details necessary for identifying eosinophils. Additionally, a convolutional block attention module (CBAM) was

inserted (P2 level in Figure S1) to refine feature representations by emphasizing spatial and channelwise distinctions[17]. This attention mechanism helps the network better distinguish eosinophils from the surrounding background tissue and other cellular structures.

The neck of the model was redesigned using a bidirectional feature pyramid network (BiFPN), which allows for the efficient fusion of multiscale features across different levels of resolution[18]. Unlike conventional architectures that rely solely on top-down or bottom-up pathways, BiFPN enables bidirectional information flow, allowing the network to adaptively emphasize features that are most relevant to the detection task. This structure facilitates the integration of fine-grained spatial information from early layers with the semantic context captured in deeper layers, thereby supporting the consistent identification of eosinophils across a wide range of sizes, shapes, and staining intensities.

At the end of the network, which refers to the detection layer, conventional YOLO models perform detection across multiple scales (P3–P5 in Figure S1); however, our model extends this strategy by incorporating higher-resolution feature levels (P1 and P2 in Figure S2) into the detection head. This extended multiresolution design enhances sensitivity to small and densely clustered eosinophils, allowing for more precise localization in histological images. By combining fine spatial details from early layers with semantic context from deeper layers, the model achieves consistent detection performance across diverse tissue conditions.

Statistical Analysis

The relationship between the deep learning-based tissue eosinophil count and the JESREC score was assessed by Pearson correlation[19]. Univariate logistic regression was performed to evaluate whether both scores were associated with the final diagnosis of ECRS.

Receiver operating characteristic (ROC) curves were constructed to assess the diagnostic potential of deep learning-based tissue eosinophil estimation. ROC curve analysis was successful if the clinical diagnostic method resulted in the same result as the gold standard, which was ECRS if the tissue eosinophil count was greater than 10/HPF. Statistical analyses were performed utilizing SPSS 30 for Windows (SPSS Inc., Chicago, IL, USA). $p < 0.05$ was considered to indicate statistical significance.

Declarations

Author contributions statement

J.Y.L. conceived the study. J.Y.L. and H.J.K. developed the methodology and performed the formal analysis. J.Y.L., D.J., and H.J.K. curated the data. H.J.K., K.H.P., and S.C.L. prepared the visualizations. D.H.K. and S.C.L. supervised project administration. J.Y.L., D.H.K., and S.C.L. acquired funding. J.Y.L. and H.J.K. wrote the original draft. J.Y.L., H.J.K., and D.J. reviewed and edited the manuscript. All authors reviewed and approved the final manuscript.

Additional information

The datasets used and/or analysed during the current study available from the corresponding author on reasonable request. The authors declare no competing interests.

Funding

This study was supported by a grant of the Korea Health Technology R&D Project through the Korea Health Industry Development Institute (KHIDI), funded by the Ministry of Health & Welfare, Republic of Korea (RS-2025-25468047), the E.N.T. Fund of the Catholic University of Korea made in the program year of 2025 (52025B000100027), and the National Research Foundation of Korea (NRF) grant funded by the Korea government (MSIT)(RS-2023-00209494). The sponsors had no role in the study design, data collection and analysis, decision to publish, or preparation of the manuscript.

Author Contribution

J.Y.L. conceived the study. J.Y.L. and H.J.K. developed the methodology and performed the formal analysis. J.Y.L., D.J., and H.J.K. curated the data. H.J.K., K.H.P., and S.C.L. prepared the visualizations. D.H.K. and S.C.L. supervised project administration. J.Y.L., D.H.K., and S.C.L. acquired funding. J.Y.L. and H.J.K. wrote the original draft. J.Y.L., H.J.K., and D.J. reviewed and edited the manuscript. All authors reviewed and approved the final manuscript.

Data Availability

The datasets generated and/or analysed during the current study are available from the corresponding author on reasonable request.

References

1. Del Pozo, V. et al. Expert consensus on the use of systemic glucocorticoids for managing eosinophil-related diseases. *Front. Immunol.* **14**, 1310211 (2024).
2. Hellings, P. W. et al. EUFOREA/EPOS2020 statement on the clinical considerations for chronic rhinosinusitis with nasal polyps care. *Allergy* **79**, 1123–1133 (2024).
3. McHugh, T., Snidvongs, K., Xie, M., Banglawala, S. & Sommer, D. High tissue eosinophilia as a marker to predict recurrence for eosinophilic chronic rhinosinusitis: a systematic review and meta-analysis in International forum of allergy &. *rhinology* 1421–1429 (2018). (Wiley Online Library.
4. Greeley, C., Holder, L., Nilsson, E. E. & Skinner, M. K. Scalable deep learning artificial intelligence histopathology slide analysis and validation. *Sci. Rep.* **14**, 26748 (2024).

5. Liu, Y. et al. Artificial intelligence–based breast cancer nodal metastasis detection: insights into the black box for pathologists. *Arch. Pathol. Lab. Med.* **143**, 859–868 (2019).
6. Ström, P. et al. Artificial intelligence for diagnosis and grading of prostate cancer in biopsies: a population-based, diagnostic study. *Lancet Oncol.* **21**, 222–232 (2020).
7. Wang, S. et al. Artificial intelligence in lung cancer pathology image analysis. *Cancers* **11**, 1673 (2019).
8. Vande Casteele, N. et al. Utilizing deep learning to analyze whole slide images of colonic biopsies for associations between eosinophil density and clinicopathologic features in active ulcerative colitis. *Inflamm. Bowel Dis.* **28**, 539–546 (2022).
9. Lee, J. Y. et al. Diagnostic criteria for eosinophilic chronic rhinosinusitis: Comparative analysis and novel scoring system. *Int. Forum Allergy Rhinology*. **14**, 1746–1756 (2024).
10. Lee, J. Y., Ali, A., Kim, M., Kim, S. W. & S. W. & Fractional Exhaled Nitric Oxide for Diagnosing Eosinophilic Chronic Rhinosinusitis: A Systematic Review and Meta-analysis. *Otolaryngology–Head Neck Surg.* **174**, 593–600 (2026).
11. Fokkens, W. et al. EPOS/EUFOREA update on indication and evaluation of Biologics in Chronic Rhinosinusitis with Nasal Polyps 2023. *Rhinology* **61**, 194–202 (2023).
12. Deems, D. A. et al. Smell and taste disorders, a study of 750 patients from the University of Pennsylvania Smell and Taste Center. *Archives otolaryngology–head neck Surg.* **117**, 519–528 (1991).
13. Doty, R. L. & Marcus, A. William Lee, W. Development of the 12-item cross-cultural smell identification test (CC-SIT). *Laryngoscope* **106**, 353–356 (1996).
14. Lund, V. J. & Mackay, I. S. Staging in rhinosinusitis. *Rhinology* **31**, 183–183 (1993).
15. Sakuma, Y. et al. New clinical diagnostic criteria for eosinophilic chronic rhinosinusitis. *Auris Nasus Larynx*. **38**, 583–588 (2011).
16. Woo, S., Park, J., Lee, J. Y., Kweon, I. S. & Cbam Convolutional block attention module in Proceedings of the European conference on computer vision (ECCV) 3–19 (2018).
17. Tan, M., Pang, R., Le, Q. V. & Efficientdet Scalable and efficient object detection in Proceedings of the IEEE/CVF conference on computer vision and pattern recognition 10781–10790 (2020).
18. Liu, S., Qi, L., Qin, H., Shi, J. & Jia, J. Path aggregation network for instance segmentation in Proceedings of the IEEE conference on computer vision and pattern recognition 8759–8768 (2018).
19. Tokunaga, T. et al. Novel scoring system and algorithm for classifying chronic rhinosinusitis: the JESREC Study. *Allergy* **70**, 995–1003 (2015).
20. Wang, K. et al. Deep learning-based prediction of treatment prognosis from nasal polyp histology slides. *Int. forum allergy rhinology* 886–898 (2023). (Wiley Online Library.
21. Wu, Q. et al. Expert-level diagnosis of nasal polyps using deep learning on whole-slide imaging. Journal of Allergy and Clinical Immunology 145, 698–701. e696 (2020).

Figures

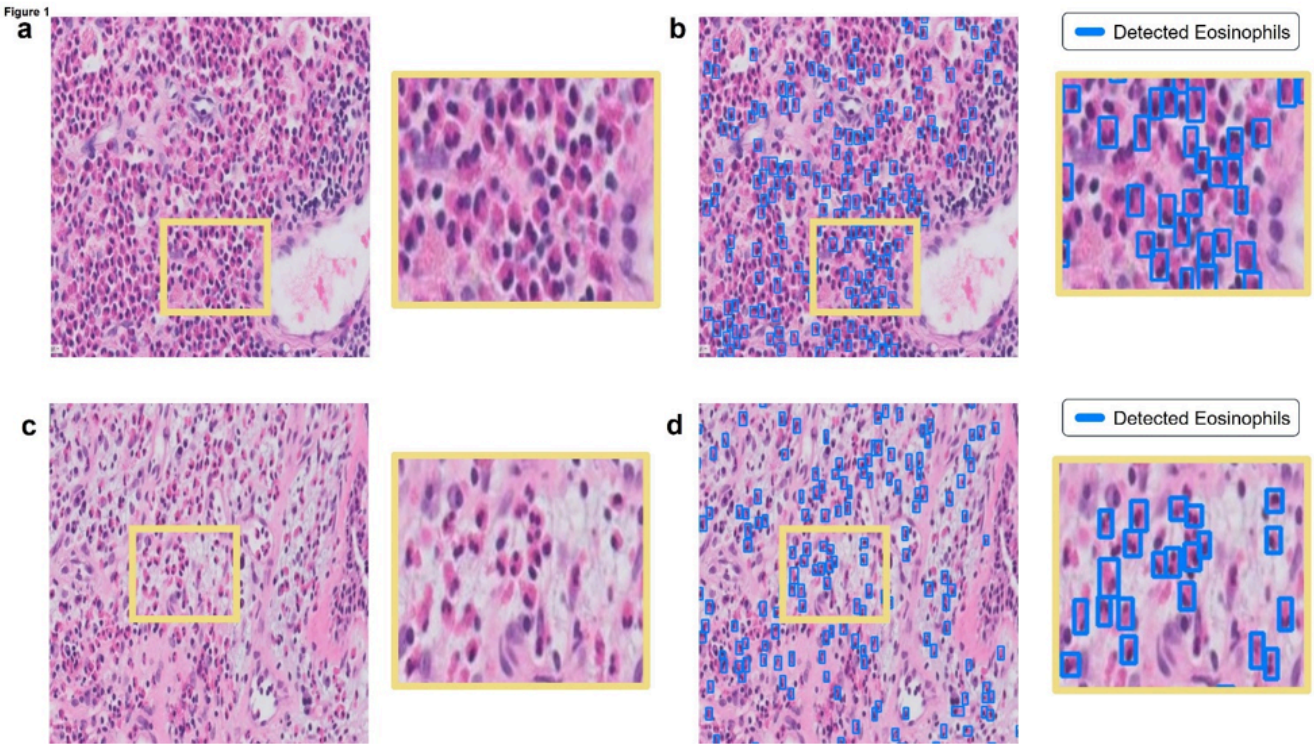


Figure 1

Eosinophil detection in dense and sparse fields. The yellow rectangle indicates the region magnified on the right. (a) Original histology image with high eosinophil density. (b) Predicted bounding boxes (blue) for the image in (a). (c) Original histology image with low eosinophil density. (d) Predicted bounding boxes (blue) for the image in (c).

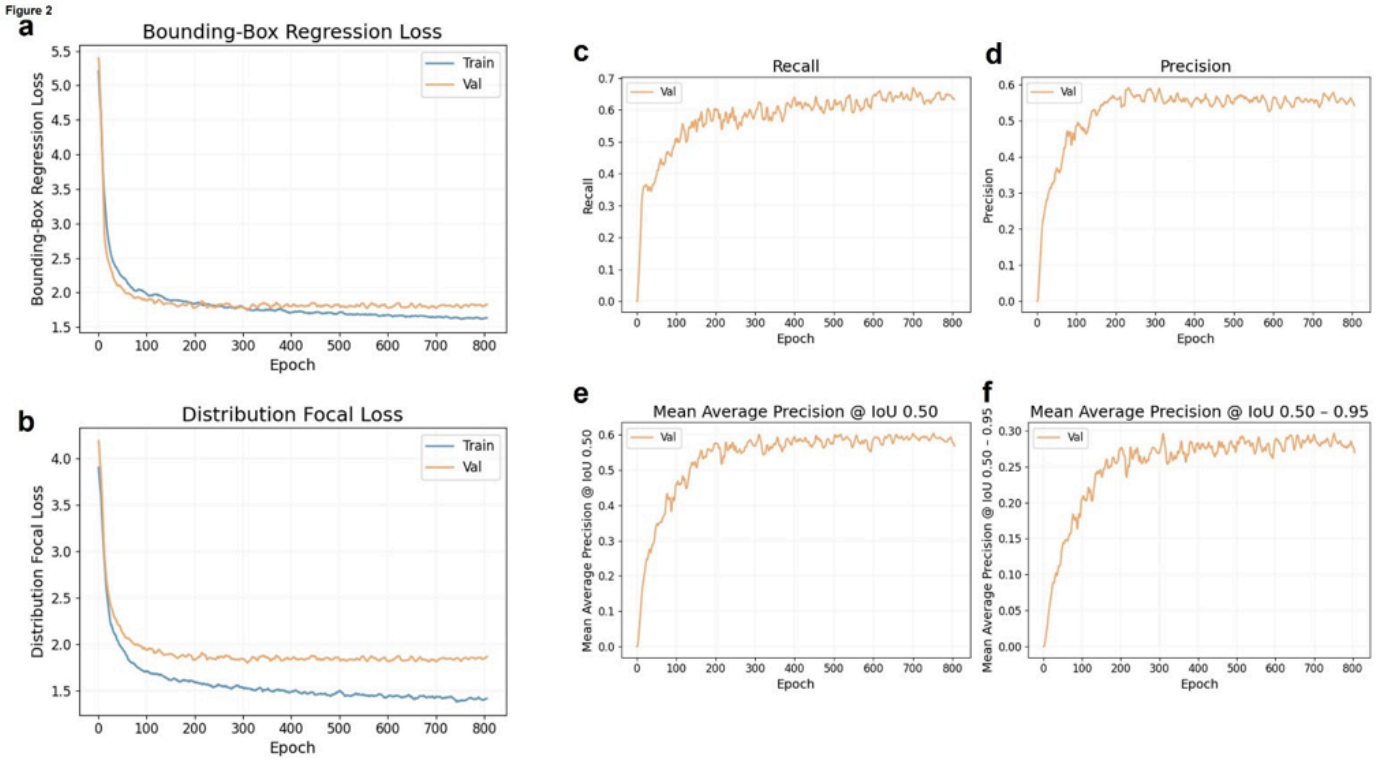


Figure 2

Training and validation curves for the EoS-YOLOv8 model. (a) Bounding-box regression loss, which measures the L1-smooth distance between the predicted and ground truth box edges; (b) distribution focal loss, which is a binwise cross-entropy that models each box edge as a discrete probability distribution to refine subpixel boundary placement; (c) recall; (d) precision; (e) mean average precision (mAP) at an intersection-over-union (IoU) threshold of 0.50; (f) mAP averaged over IoU thresholds from 0.50 to 0.95 in 0.05 increments. Metrics are plotted over 800 training epochs; the orange line represents the validation set, and the blue line represents the training set.

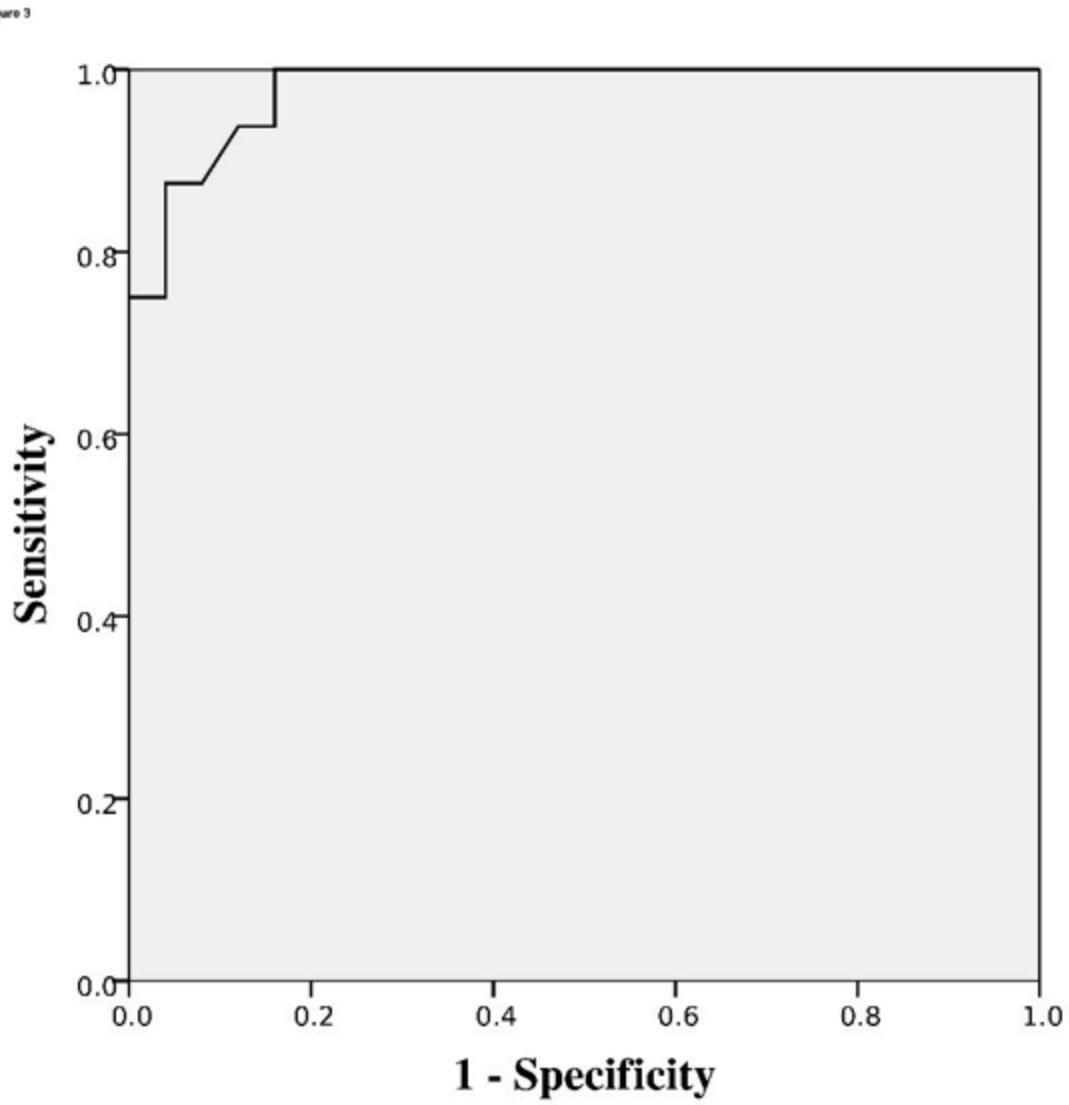


Figure 3

Receiver operating characteristic curve for the EoS-YOLOv8 model for diagnosing eosinophilic chronic rhinosinusitis in the total dataset.

Supplementary Files

This is a list of supplementary files associated with this preprint. Click to download.

- FigureS1.jpg
- FigureS2.jpg